ACS Catalysis

Research Article

pubs.acs.org/acscatalysis

# Proton-Shuttle-Assisted Heterolytic Carbon−Carbon Bond Cleavage and Formation

Jingwei Zhou,[†] Ruibo Wu,*[,†] Binju Wang,[‡] Zexing Cao,*[,‡] Honggao Yan,[§] and Yirong Mo*[,∥]

[†]School of Pharmaceutical Sciences, Sun Yat-Sen University, Guangzhou 510006, P.R. China

[‡]State Key Laboratory of Physical Chemistry of Solid Surfaces and Fujian Provincial Key Laboratory of Theoretical and Computational Chemistry, College of Chemistry and Chemical Engineering, Xiamen University, Xiamen 360015, P. R. China

[§]Center for Biological Modeling and Departments of Biochemistry and Chemistry, Michigan State University, East Lansing, Michigan 48824, United States

[∥]Department of Chemistry, Western Michigan University, Kalamazoo, Michigan 49008, United States

Supporting Information

**ABSTRACT:** The conversion of 1-deoxy-D-xylulose 5-phosphate (DXP) to 2-C-methyl-D-erythritol 4-phosphate (MEP) catalyzed by DXP reductoisomerase (DXR) is the committing step in the biosynthesis of terpenoids. This MEP pathway is essential for most pathogenic bacteria but absent in human, and thus, it is an attractive target for the development of novel antibiotics. To this end, it is critical to elucidate the conversion mechanism and identify the transition state, as many drugs are transition-state analogues. Here we performed extensive combined quantum mechanical (density functional theory B3LYP/6-31G*) and molecular mechanical molecular dynamics simulations to elucidate the catalytic mechanism. Computations confirmed the transient existence of two metastable fragments of DXP by the heterolytic C3−C4 bond cleavage, namely, 1-propene-1,2-diol and glycoaldehyde phosphate, in accord with the most recent kinetic isotope effect (KIE) experiments. Significantly, the heterolytic C3−C4 bond cleavage and C2−C4 bond formation are accompanied by proton shuttles, which significantly lower their reaction barriers to only 8.2−6.0 kcal/mol, compared with the normal single carbon−carbon bond energy 83 kcal/mol. This mechanism thus opens a novel way for the design of catalysts in the cleavage or formation of aliphatic carbon−carbon bonds.

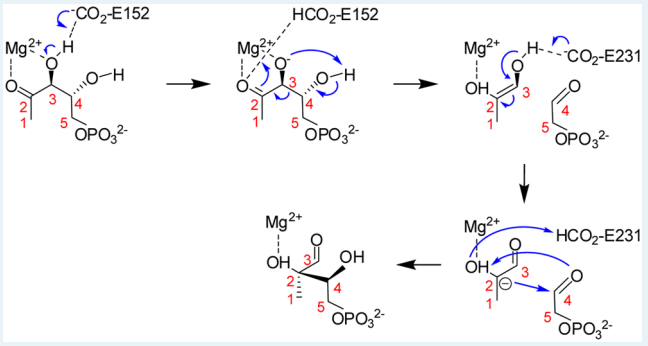


**KEYWORDS:** *carbon−carbon bond cleavage, proton shuttle, 1-deoxy-D-xylulose 5-phosphate, reductoisomerase, combined QM(DFT)/MM*

## INTRODUCTION

Infectious diseases are the leading cause of death. Due to the widespread use of antibiotics, however, pathogenic bacteria gradually acquire and spread persistent antibiotic resistance, which has become a worldwide public health-care crisis, and new targets for the development of antimicrobial agents against multidrug resistant Gram-negative bacteria such as *Pseudomonas aeruginosa* are thus urgently needed for combating the antibiotic resistance crisis. Recently, a significant target for the development of novel antibiotics has been identified in the biosynthesis of terpenoids, which are essential for all living organisms and play important roles in membrane structure, redox reactions, light harvesting, and regulation of growth and development. The significance lies in that there are two pathways for the biosynthesis of the two common five-carbon building blocks, isopentenyl diphosphate (IPP) and its isomer dimethylallyl diphosphate (DMAPP), for terpenoids, and bacteria adopt a pathway different from animals and humans.[1] The first one, or the mevalonate pathway discovered in 1950s, produces IPP from acetyl-CoA, which is converted to DMAPP by enzymatic isomerization. It is a pathway of great medical significance and is the target pathway for the class of drugs for lowering serum cholesterol. The second one, called the MEP pathway or nonmevalonate pathway or DXP pathway, was discovered and confirmed in the 1990s.[2−4] In this pathway, 1-deoxy-D-xylulose 5-phosphate (DXP) reductoisomerase (DXR) catalyzes the biosynthesis of 2-C-methyl-D-erythritol 4-phosphate (MEP), the namesake and committing step of the MEP pathway responsible for the biosynthesis of the building blocks for terpenoids in most microorganisms.[5−8] Biochemical studies have shown that the enzymatic reaction from DXP to MEP proceeds in two steps (Figure 1).[9,10] Because the MEP pathway is essential for many pathogenic microorganisms but absent in human, DXR has become an attractive target for the

Received: January 15, 2015
Revised: March 15, 2015
Published: March 19, 2015




DOI: 10.1021/acscatal.5b00079
ACS Catal. 2015, 5, 2805−2813

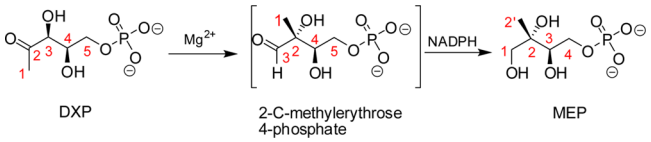


**Figure 1.** Chemical conversion from DXP to MEP catalyzed by DXR.

development of novel antibiotics, antimalarial drugs, and herbicides.

The major accomplishment so far in the studies of MEP pathway enzymes has been the structural determination, which gives a glimpse of possible reaction mechanisms and offers an opportunity for structure-based drug design.[11] With respect to DXR, atomic structures have been reported for *E. coli*, *Zymomonas mobiliz*, and *Mycobacterium tuberculosis* enzymes, abbreviated as EcDXR, ZmDXR, and MtDXR, respectively, in several liganded and apo states, highlighting the central importance of DXR as well as the friendliness of DXR to X-ray crystallographic analysis.[9,12−20] Although rich structural information on DXRs has been accumulated and available, unfortunately, the chemical mechanism of the DXR-catalyzed reaction remains unresolved and of particular the transition state of the reaction is unknown. Transition state stabilization is the hallmark of enzymatic catalysis, but the experimental determination of the transition state is challenging due to its fleeting lifetime ($\sim 10^{-13}$ s).[21] For the two steps in the DXR-catalyzed reaction (Figure 1), the first step is biologically more important and the focus of mechanistic studies, as the DXP binding site is where the antibiotics fosmidomycin binds and is considered as an attractive target for the development of new antimicrobial agents.[22] Currently, there are two possible mechanisms for the isomerization step, including the $\alpha$-ketol (**A**) and retro-aldol/aldol (**B**) mechanisms, as depicted in Figure 2.[23−27]

The main difference between them is the timing of the breaking and making of bonds. The $\alpha$-ketol mechanism is a concerted one with bond breaking (C3−C4) and making (C2−C4) occurring simultaneously, after the deprotonation of the C3 hydroxyl group. On the other hand, the retro-aldol/aldol mechanism is a stepwise one with the C3−C4 bond breaking followed by the C2−C4 bond making, in other words, there is an intermediate state with two fragments, the enolate of hydroxyacetone and the glycoaldehyde phosphate. Significant efforts have been made to identify the exact reaction mechanism via determining the kinetic isotope effects (KIEs) using $^{2}$H-, $^{13}$C- or $^{18}$O-labeled DXP as substrates, and accumulating experimental data tend to favor the retro-aldol/aldol mechanism (**B**) in which the recombination reaction, namely, the second step, is the rate-limiting step.[28−31] Still, uncertainties linger as exogenous intermediates, the enolate of hydroxyacetone and the glycoaldehyde phosphate, were not recognized and converted to MEP by DXR.[24,32,33] Even more, we note that there is no report of the direct determination of the transition state of DXP isomerization so far. Site-directed mutagenesis studies have been reported for some active site residues of EcDXR[34] and *Synechocystis* sp. PCC6803 DXR,[35,36] but how DXR stabilizes the transition state is largely unknown.

Complementarily, computational studies have the potential and flexibility to correlate the structures, dynamics and functions of enzymes, as molecular dynamics simulations of enzymes at the atomic level can reveal the dynamic behavior of enzymes in catalytic processes and provide insights into the reaction mechanisms and the physical principles underlying these processes. As the catalytic power and specificity of enzymes largely come from the overall enzyme and solvation environment, it is critical to consider the whole enzyme system in calculations to probe the catalytic mechanism.[37−41] Molecular dynamics simulations with the combined QM/MM methods can provide the details related to the catalytic activities and reaction mechanisms.[42] For instance, although site-directed mutagenesis and KIE experiments afford important information on the reaction mechanism and the role of residues in the active site, interpretation of these experimental data requires theoretical studies to elucidate the energetics of enzyme catalysis. We note that a similar enzyme, acetohydroxy acid isomeroreductase, which catalyzes the transformation of 2-aceto-lactate or 2-aceto-2-hydroxybutyrate into 2,3-dihydroxy-3-isovalerate or 2,3-dihydroxy-3-methylvalerate, has been computationally studied by Martin et al. using combined QM(AM1)/MM molecular dynamics simulations.[43] Here we performed extensive Born−Oppenheimer DFT combined quantum mechanical and molecular mechanical (in short QM(B3LYP/6-31G*)/MM) molecular dynamics simulations of the DXP isomerization in an attempt to determine the chemical mechanism of the EcDXR-catalyzed reaction and its transition state as well as to investigate the roles of active site residues in catalysis.

## 1. METHODOLOGY

**1.1. Initial Construction of the Simulated System.** Because the primary goal of our QM/MM study is to determine the transition state of the DXP isomerization, computations will begin with the Michaelis complex of the enzymatic reaction. In general, the structure of a Michaelis complex is not experimentally available, as the Michaelis complex is not stable enough for structural determination.

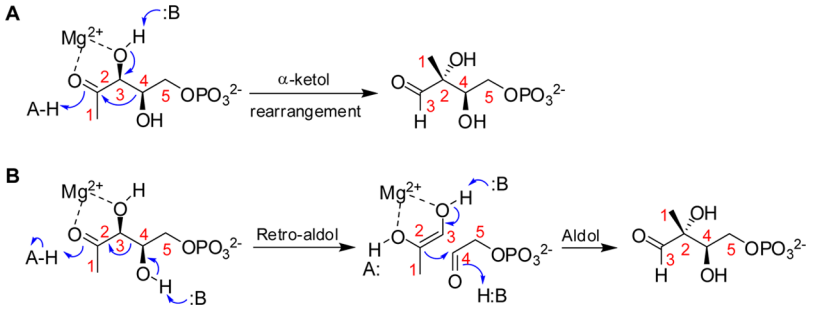


**Figure 2.** Proposed the $\alpha$-ketol (**A**) and the retro-aldol/aldol (**B**) mechanisms for the isomerization of DXP to the intermediate 2-*C*-methylerythrose 4-phosphate.



DOI: 10.1021/acscatal.5b00079
*ACS Catal.* 2015, 5, 2805−2813

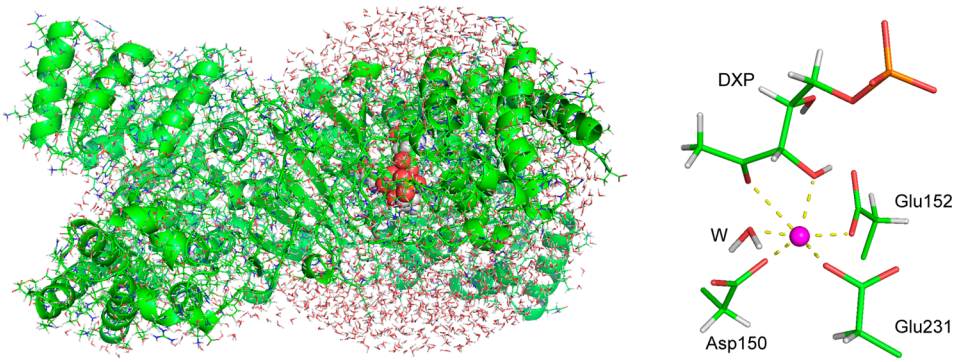


**Figure 3.** (a) QM(DFT)/MM molecular dynamics simulation model for the Michaelis complex of DXR, DXP, NADPH, and $Mg^{2+}$, where the active site is highlighted in space-filling mode; (b) QM part in the combined QM(DFT)/MM simulations.

Consequently, a model for the Michaelis complex has to be constructed in silico, and the model construction is critical for a successful computational simulation, as the time scale for such a simulation is generally insufficient for modeling large conformational changes.

Although the reduction reaction follows the isomerization reaction (Figure 1), NADPH has to be present for the DXP isomerization, and therefore, the Michaelis complex has the following essential composition: DXR, NADPH, DXP, and $Mg^{2+}$ (or other active divalent metal ions such as $Mn^{2+}$ and $Co^{2+}$). EcDXR is an excellent system for the simulation, because among the 10 published crystal structures, three structures have a composition very similar to that of the Michaelis complex. One structure (PDB code: 1Q0Q) contains both substrates NADPH and DXP,[14] another (PDB code: 1Q0L) contains NADPH and the inhibitor fosmidomycin,[14] and the third (PDB code: 2EGH) contains NADPH, fosmidomycin, and $Mg^{2+}$.[18] Therefore, one can construct a model of the Michaelis complex from 1Q0Q by adding a $Mg^{2+}$ ion or from 2EGH by mutating fosmidomycin, which is very similar to DXP. Upon a close examination, however, we found that the protein conformation of 2EGH is essentially the same as that of the binary complex with NADPH (PDB code: 1JVS),[9] which is an open conformation, presumably because the crystals of the quaternary complex were obtained by soaking the crystals of the binary NADPH complex with $Mg^{2+}$. Thus, the value of the structure 2EGH lies in providing the bound $Mg^{2+}$ coordination chemistry.

The structure of the ternary substrate complex 1Q0Q, which was obtained by cocrystallization and also happened to have the best resolution (1.9 Å), is an excellent starting point for the construction of the Michaelis complex. The only missing component is $Mg^{2+}$. The structure is in a close conformation presumably required for catalysis with the fixation of the phosphate function of DXP.[9] Although a divalent metal ion is required for catalysis, it does not appear that the metal ion has major effects on the protein conformation, as the protein conformation of the ternary substrate complex of EcDXR (without the metal ion) is very similar to that of the quaternary complex of MtDXR in complex with NADPH, fosmidomycin, and $Mn^{2+}$ (PDB code: 2JCZ).[13] We have inserted a $Mg^{2+}$ ion and a coordinating water molecule into 1Q0Q by superimposing the key residues (Asp150, Glu152, Ser186, His209, and Glu231) of the structures 1Q0Q and 2EGH. The resulting $Mg^{2+}$ has the full octahedral coordination, very similar to that obtained by superposition of the EcDXR structure 1Q0Q and the MtDXR structure 2JCZ. We choose $Mg^{2+}$ instead of $Mn^{2+}$ as the metal ion in the computational model because the former is more relevant in vivo.[44−46] Although both chains (chain A and chain B) of complex were retained in our computational simulations, the chain A was chosen for reaction mechanism study. The protonation states of charged residues were first determined via H++ program,[47] followed by individual examinations of the niches of each key residues. Asp150, Glu152, and Glu231 were deprotonated as negative charge centers to form coordination bonds with the magnesium ion. Lys125, which is not in immediate contact with DXP, was designated neutral as initially we thought that it might be a general base to deprotonate the hydroxyl group at C3 of XDP, but later test computations did not support this assumption. Lys228 was protonated and thus carried a positive charge. Several $Na^{+}$ ions were added around the protein surface to neutralize the total charges for the complex. Finally, the whole system was solvated into a cubic water box with a 6 Å distance between the solvent box wall and the nearest solute atoms.

**1.2. Final Setup of the Simulated System.** With the complete DXR-DXP complex solvated in a cubic water box, a few steps of minimization and equilibrium were taken for the whole system at the classical molecular mechanical (MM) level. The TIP3P model[48] and Amber99SB force field[49−51] were employed for the water and protein respectively, whereas the force field parameters of DXP was generated from AMBER GAFF force field.[52] The partial atomic charges of DXP were obtained from the restrained electrostatic potential (RESP) method based on the HF/6-31G* calculation. Preliminary computational simulations reported in this work were performed with the AMBER12 package.[53]

The energy minimization of the solvated DXR-DXP system was performed in order to remove bad contacts and relax the system. After several iterations of minimization, the heating MD simulation was performed with the temperature gradually increasing from 0 to 300 K under the NVT ensemble for 50 ps. Afterward, 100 ps MD simulations were performed under the NPT ensemble to relax the system density to be about 1.0 g/$cm^3$, with the target temperature of 300 K and the target pressure of 1.0 atm. At last, the system was further equilibrated for ∼10 ns. The resulting conformations were taken for subsequent calculations at the QM(DFT)/MM theoretical level. During the present MM molecular dynamics simulations, the SHAKE algorithm was applied to constrain all hydrogen-


DOI: 10.1021/acscatal.5b00079
ACS Catal. 2015, 5, 2805−2813

containing bonds with a tolerance of $10^{-5}$.[54] The Berendsen thermostat[55] method was used to control the system temperature, and a cutoff of 12 or 18 Å was set for either van der Waals or electrostatic interactions.

**1.3. Born−Oppenheimer QM(DFT)/MM Molecular Dynamics Simulations.** As demanded by the viable mechanisms, the DXP isomerization involves general acid/base catalysis. Although the $Mg^{2+}$ ligands (Asp150, Glu152, and Glu231) are known, the identities of the general base and/or acid are not certain. However, the residues involved in the general acid/base catalysis must be close to the hydroxyl groups of the bound DXP. According to the 1Q0Q crystal structure, the residues that are most likely involved in the general acid/base catalysis are Glu152 and Glu231. The distance of the carboxylate group (OE2) of Glu152 to the 4-hydroxyl oxygen is 2.50 Å, whereas the distance between OE2 of Glu231 and the C-3 hydroxyl oxygen is 2.63 Å. As such, our QM region consists of DXP, side chains of amino acid residues Asp150, Glu152, and Glu231, $Mg^{2+}$, and the water molecule coordinated with $Mg^{2+}$. NADPH is not directly involved in the first isomerization step, so it is not included in the QM region.

The DXR-DXP complex from the above MD simulations at the MM level was cut into a sphere by removing the solvent water molecules which were beyond 30 Å of the $Mg^{2+}$ ion in the active site of chain A. Figure 3 shows the final computational model for the QM(B3LYP/6-31G*)/MM molecular dynamics simulations, which were performed with the integrated Q-Chem/Tinker package.[56,57] The QM/MM boundaries were described by the pseudobond approach with the improved pseudobond parameters developed by Zhang and co-workers.[58,59] For all QM/MM calculations, the spherical boundary condition was applied and the atoms beyond 24 Å away from the central $Mg^{2+}$ ion of chain A were fixed. Within the MM region, the 18 and 12 Å cutoffs were employed for electrostatic and van der Waals interactions, respectively. There was no cutoff for electrostatic interactions between QM and MM regions. The overall QM/MM systems were once again minimized for several iterations, followed by ∼5 ps QM/MM molecular dynamics simulations with the time step of 1 fs and the Beeman algorithm[60] to integrate the Newton equations of motion, as well as the Berendsen thermostat method[55] to control the system temperature at 300 K. The resulting conformation was then minimized to map out the energy paths (as close as possible to the minimum ones) with reaction coordinate driving method.[61] For each determined structure along the energy paths, the MM subsystem, which accounts for the majority of the whole system, was equilibrated with 500 ps molecular dynamics simulations with the QM subsystem fixed. With this equilibrated conformation as the starting structure, 20 ps QM(DFT)MM molecular dynamics simulations with umbrella sampling[62,63] were finally carried out. A total of 1500 configurations of the last 15 ps at each window were collected for data analysis. The probability distributions along the reaction coordinate were determined for each window and pieced together with the WHAM[64,65] to yield the reaction free energy profile. Statistical analyses for errors were also carried out from the last 15 ps data.

## 2. RESULTS AND DISCUSSION

**2.1. Substrate Binding.** After the initial construction and MD simulations at the MM level, followed by the final setup and conformational equilibrium at the QM(DFT)/MM level, we obtained the stable Michaelis complex of DXR, DXP, NADPH, and $Mg^{2+}$ at room temperature. A snapshot of the reactive site at this equilibrium state is shown in Figure 4. It has been known that the small ionic radius of $Mg^{2+}$ together with its strong binding capability to hydroxyl and carboxylate groups result in unusually strong oxygen−magnesium bonds. In the present case, we identified six coordinating ligands. Apart from the carboxylate groups of Asp150, Glu152, and Glu231 and the water molecule which binds to $Mg^{2+}$ in the monodentate mode, the substrate DXP provides two oxygen ligands (O2 and O3) and binds to the divalent metal cation in a bidentate mode. The binding distances for the binding state **R** are listed in Table S1 (Supporting Information). It is seen that the interaction between the DXP O2 and the metal ion is relatively weak due to the longer distance with increased uncertainty than the rest O−Mg bonds.

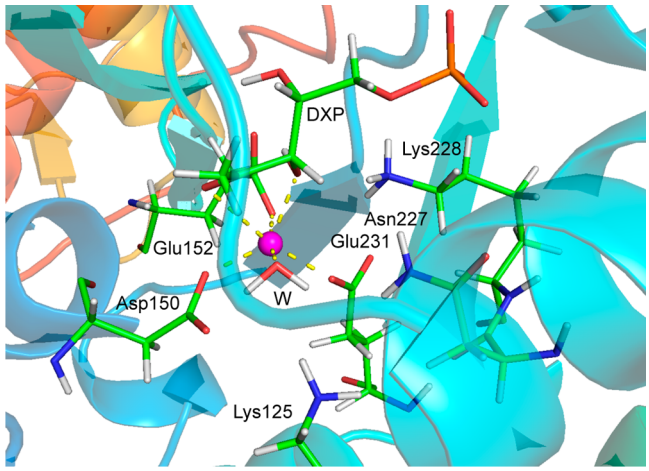


**Figure 4.** Representative structure for the Michaelis complex of DXR, DXP, NADPH, and $Mg^{2+}$ at equilibrium state at room temperature.

**2.2. Deprotonation of DXP.** The above equilibrium conformation shows that both the hydroxyl groups at C3 and C4 are close to the carboxylate group of Glu152, which plays the key role as the general base in this enzyme. In accord with the crystal structure 1Q0Q,[14] Glu152 is the nearest possible base for either C3 or C4 hydroxyl group, and further structural analysis shows that the hydroxyl group at C3 is well positioned toward the carboxylate group of Glu152 with a H(O3)···O distance about 1.9 Å. On the other hand, the hydroxyl group at C4 forms a hydrogen bond with a surrounding water molecule (which bonds to the carbonyl oxygen O2 of Glu152, as well as another outer water molecule). The distance between H(O4) and the carboxylate group of Glu152 is about 2.9 Å. Other candidates of the general base are Asp150 and Glu231, but the protons of the hydroxyl groups are a considerable distance away (more than 4 Å) from the negatively charged oxygen atoms.

It has been hypothesized that the $\alpha$-ketol mechanism is initiated by the deprotonation of the C3 hydroxyl group of DXP, whereas the retro-aldol/aldol mechanism is initiated by the deprotonation of the C4 hydroxyl group (Figure 2). As such, we started the computational exploration of the reaction mechanism by deriving the energy profile for the proton transfer from the C4 site. The reaction coordinate for the energy profile is defined as the distance difference between the H(O4)···O(Glu152) bond and the O4−H bond. QM(DFT)/MM MD simulation results (Figure S1a) show that the deprotonation involves two steps, and the first step with a barrier of only ∼4 kcal/mol concerns the rotation of the


DOI: 10.1021/acscatal.5b00079
ACS Catal. 2015, 5, 2805−2813

hydroxyl group to move its hydrogen H(O4) toward Glu152 by breaking the hydrogen bond with the adjacent water molecule and forming a new hydrogen bond with Glu152. Thus, the first step can be regarded as a preparation step, and **R′** is the "true" initial state for the subsequent proton transfer, which has a reaction barrier of 11.5 kcal/mol. Once the proton is transferred, the system is gradually stabilized and reaches the intermediate state **INT1**. **INT1** and **R′** states have comparable energies. This is in agreement with the computational study of *Mycobacterium tuberculosis* DXR with the empirical valence bond method by Henriksson et al., who showed that the environment of enzyme reduces the p$K_a$ difference between Glu153 (Glu152 in EcDXR) and 4-hydroxyl of DXP by about 7 p$K$ units, making the proton transfer nearly isoergonic.[13] Figure S2 shows the snapshots of **R′** and **INT1** together with the transition state **TS1′**. Surprisingly, both structures of **TS1′** and **INT1** show that accompanied by the proton transfer from C4-OH to Glu152, simultaneously there is an intramolecular proton transfer from C3-OH to C4-$O^-$. In the end, the proton gained by Glu152 seems from C3-OH instead of C4-OH. This is understandable as the former has a much higher acidity than the latter as the former is bound to a divalent metal ion. This raises a question whether the proton transfer is more efficient directly from the hydroxyl group at the C3 site than from the C4-hydroxyl group to Glu152. QM(DFT)/MM MD simulations (Figure S1b and Figure 5) confirmed that this is indeed

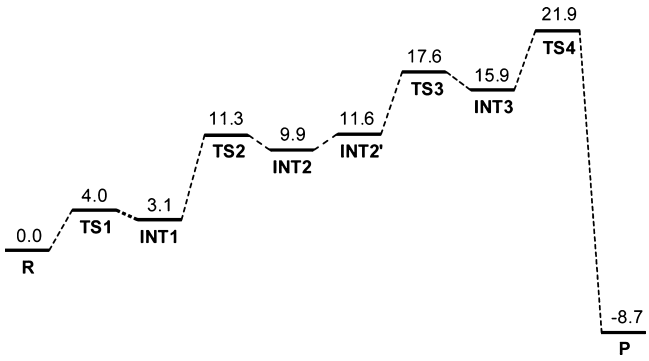


**Figure 5.** Overall energy profile in kcal/mol for the isomerization of DXP (**R**) to the intermediate 2-C-methylerythrose 4-phosphate (**P**), catalyzed by DXR.

the case as the reaction barrier for the proton transfer from C3-OH to Glu152 is only 4.0 kcal/mol and the product of the proton transfer is the very same **INT1**. We note that at **INT1**, although the divalent metal ion $Mg^{2+}$ maintains an octahedral coordination mode, the carbonyl oxygen O2 of DXP is still about ∼2.85 Å away and forms a hydrogen bond with a surrounding water molecule (see Table S1). Yet the hydroxyl O4 shows no propensity to replace O2 to bind the metal ion. This challenges the claim of the C3−C4 binding mode of DXP.[24,66]

**2.3. Cleavage of the C3−C4 Bond.** In the isomerization of DXP to 2-C-methylerythrose 4-phosphate, the key step is the aliphatic carbon−carbon bond breaking and formation. Whether there are stable intermediates, namely, the enolate of hydroxyacetone and the glycoaldehyde phosphate, is the focal point for the overall reaction mechanism. To follow the reaction trajectory, we simply define the reaction coordinate with the C3−C4 bond distance, and we examine the energetic and conformational evolutions along the stretching of this bond (Figure S3, also see Figure 5). At the QM(DFT)/MM theoretical level, the reaction barrier for the bond breaking from **INT1** to **TS2** is only 8.2 kcal/mol, suggesting the extremely high rate constant ($6.0 \times 10^6$ $s^{-1}$ based on Eyring's transition state theory) for this process. For comparison, the standard C−C single bond energy is 83 kcal/mol (corresponding to a rate constant $9.0 \times 10^{-49}$ $s^{-1}$). Note that at the transition state (**TS2**), the C3−C4 bond distance is around 2.13 Å, profoundly longer than any normal C−C single bond (1.54 Å). After overcoming the barrier, the system gets into an intermediate state (**INT2**), which is metastable and has a high tendency to go back to the initial state **INT1**. The energy profile around **INT2** is quite flat, suggesting that the broken fragments have the freedom to move around to certain extent. Snapshots of QM region together with the surroundings of the DXP molecule (or its fragments) at **TS2** and **INT2** are shown in Figure 6.

The QM region in Figure 6 shows that the very low reaction barrier from **INT1** to **TS2** for the C3−C4 single bond breaking benefits from a series of simultaneous processes. On one hand, with the stretching of the C3−C4 bond, there is an instantaneous proton transfer from the hydroxyl group at C4 to the hydroxyl anion at C3 (as shown in Figure 6a), whose proton is lost to Glu152 in the previous deprotonation step. With the protonation at O3, the binding between O3 and $Mg^{2+}$ is weakened (the O2···$Mg^{2+}$ distance is stretched from 2.16 Å at **INT1** to 2.36 Å at **TS2**, see Table S1), and consequently, O2 (rather than O4) moves to $Mg^{2+}$ and subsequently DXP reinforces the C2−C3 binding mode (the O2···$Mg^{2+}$ distance is shortened from 2.85 Å at **INT1** to 2.17 Å at **TS2**) and $Mg^{2+}$ is in a perfect octahedral coordination again. This leaves the gradual formation of a carbonyl group at C4 and subsequently the glycoaldehyde phosphate. On the other hand, the protonated Glu152 serves as a general acid and provides a proton to the now negatively charged hydroxyacetone enolate, or more specifically to O2, leading to 1-propene-1,2-diol which is stabilized by the divalent metal ion. At the **INT2** state, 1-propene-1,2-diol binds to $Mg^{2+}$ with O2, and the hydroxyl group at C3 rotates to break the binding with $Mg^{2+}$ and form a strong hydrogen bond with Glu231. To maintain the favorable octahedral coordination, $Mg^{2+}$ binds both carboxylate oxygen atoms of Asp150. The hydroxyl hydrogen at C2, however, still bonds to the carboxylate group of Glu152. There is also a hydrogen bond between the C3-hydroxyl group and Glu231. To gain insights into this series of sequential processes (the cleavage of the C3−C4 bond, two proton transfers and the formation of C2═C3 double bond), we plot the variations of the C2−C3 (Figure S4a) and relevant O−H bond distances (Figure S5) along the breaking of the C3−C4 bond (reaction coordinate). Notably, the trajectories of the distances between the transferred protons and their donors/acceptors, manifest that the two proton transfers are sequential rather than concurrent, as the proton transfer from the C4-hydroxyl group to O3 occurs at RC = 1.85−2.20 Å, whereas the proton transfer from the deprotonated Glu152 to O2 occurs at RC = 2.5−2.6 Å. We reinforce that these proton transfers occur spontaneously with the breaking of the C3−C4 bond, so is the formation of the carbon−carbon double bond, and we did not impose any constraint on these processes. Overall the reaction barrier is only 8.2 kcal/mol.

As the central focus of the present work is on the reaction mechanism and the transition state conformation, it is valuable to scrutinize how the enzyme stabilizes the transition state by


DOI: 10.1021/acscatal.5b00079
ACS Catal. 2015, 5, 2805−2813

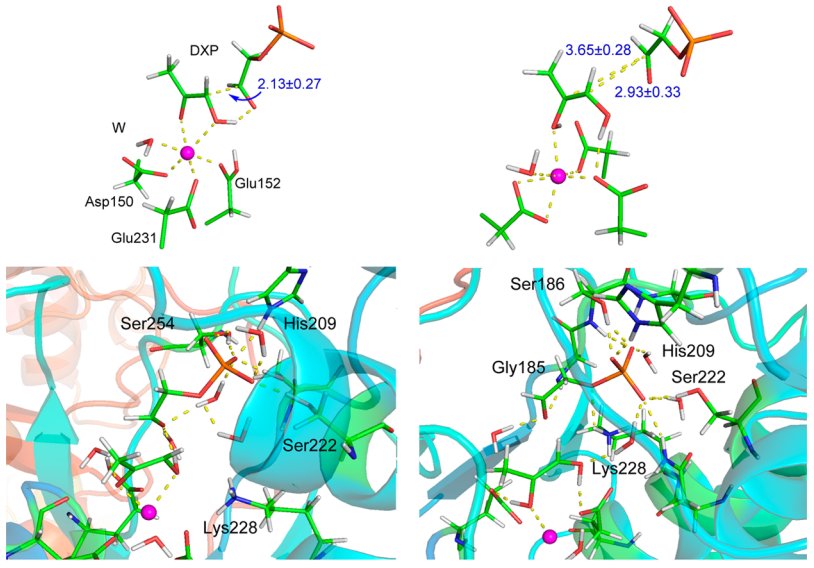


(a) TS2 (b) INT2

**Figure 6.** Snapshots of the key structures of (a) the transition state and (b) the intermediate product showing the QM region (up) and the amino acids surrounding DXP (below) in the C3−C4 bond-breaking process.

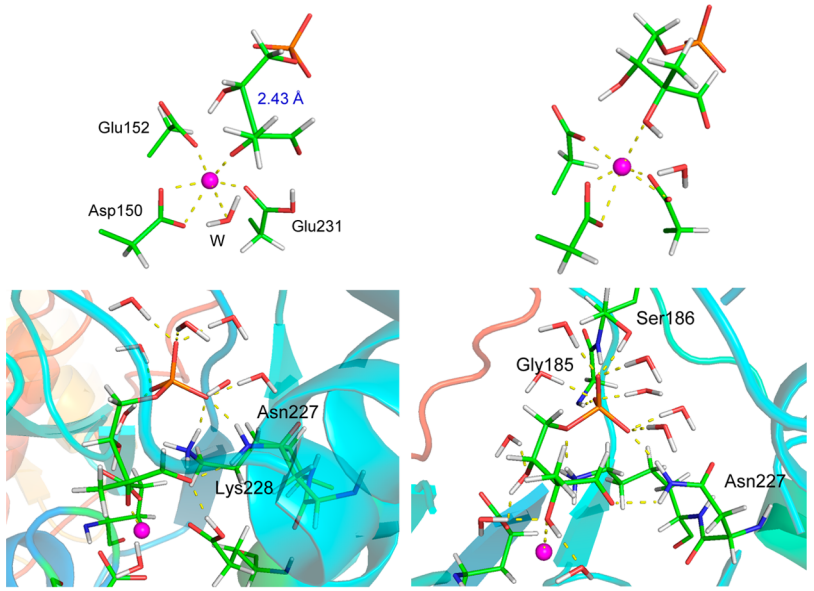


(a) TS4 (b) P

**Figure 7.** Snapshots of the key structures (a) **TS4** and (b) **P** showing the QM region (up) and the amino acids surrounding the product 2-*C*-methylerythrose 4-phosphate (below) in the C2−C4 single bond formation.

identifying the important amino acid (Figure 6). At the transition state **TS2**, His209, Ser222, and Ser254, together with two water molecules, stabilize the negatively charged phosphate group, while the carbonyl group at C4 is strongly bound by the hydroxyl group at C3, although two water molecules also form hydrogen bonds with the carbonyl oxygen O4. The strong hydrogen bond O4···H−O3 prevents the possible oxygen exchange of O4 with water molecules at the transition state. Apart from $Mg^{2+}$, the hydroxyl group at C3 is stabilized by Lys228. At the product state **INT2** of the C3−C4 bond-breaking step, Lys228, Gly185 (with its NH group) together with one water hold carbonyl O4. Ser222, His209, Ser186 with both OH and main-chain NH groups, Gly with its NH group plus a couple of water molecules trap the phosphate group. 1-Propene-1,2-diol is monodentate to $Mg^{2+}$ with O2, and Asp150 now is bidentate to the metal ion. H-O3 is stabilized by Glu231 and one water molecule, while O2-H forms a hydrogen bond with Glu152.

One rising question is whether the carbonyl oxygen at C4 in the glycoaldehyde phosphate has a chance to exchange with water oxygen. The answer should be no as it is trapped by the hydrogen bonds with the main chain −NH group of Gly185 and the $-NH_3^+$ group of Lys228, apart from a hydrogen bond with one water molecule around. This is confirmed experimentally.[31]

### 2.4. Formation of 2-*C*-Methylerythrose 4-Phosphate.

So far we have confirmed the metastable existence of DXP fragments, the glycoaldehyde phosphate and 1-propene-1,2-



DOI: 10.1021/acscatal.5b00079
*ACS Catal.* 2015, 5, 2805−2813

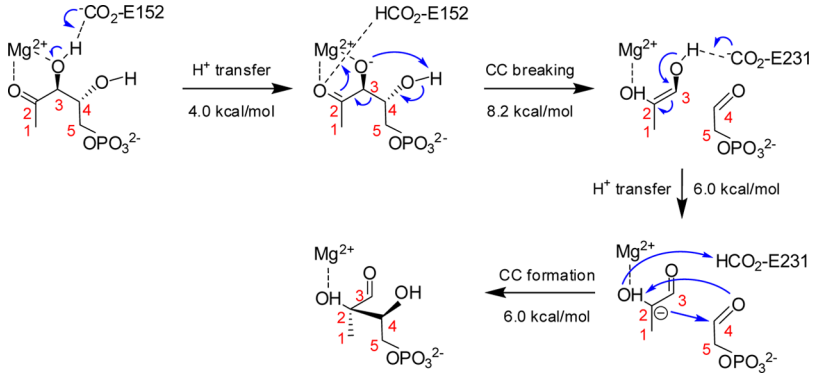


**Figure 8.** Mechanism for the isomerization of DXP to the intermediate 2-*C*-methylerythrose 4-phosphate with reaction barriers based on the present QM(DFT)/MM molecular dynamics simulations.

diol. To link them together with a new C2−C4 bond, we need generate a nucleophilic center at the C2 site of 1-propene-1,2-diol which subsequently can attack the carbon site of the carbonyl group at the glycoaldehyde phosphate. To this end, there should be a deprotonation from the hydroxyl group at C3 which makes C2 partially negatively charged. At the **INT2** state (Figure 6b), we have observed that the hydroxyl group at C3 forms a strong hydrogen bond with the carboxylate group of Glu231. Thus, Glu231 most likely acts as the Lewis base to remove the proton from the hydroxyl group. By defining the reaction coordinate as the difference of the bond distances of the transferred proton with O3 and the carboxylate oxygen of Glu152 which is not bound to $Mg^{2+}$, we derived the energy profile (Figure S6a and Figure 5). Much like the early deprotonation step in Figure S1a, the preliminary step from **INT2** to **INT2′** with a barrier of ∼1.8 kcal/mol corresponds to the orientation adjustment of the hydroxyl group, and **INT2′** thus should be regarded as the true beginning state for the subsequent proton transfer, which has a barrier of 6.0 kcal/mol. Although this proton transfer step can proceed efficiently, it is endothermic. Snapshots of key structures **INT2′** → **TS3** → **INT3** can be seen in Figure S7. In this process, 1-propene-1,2-diol and its deprotonated form maintain monobinding mode with the hydroxyl group at C2. The glycoaldehyde phosphate is not involved in the reaction and acts as a spectator and moves around to certain extend, with bonding with surrounding groups and solvent molecules little changed.

With the C2 site at the deprotonated 1-propene-1,2-diol now negatively charged, it is ready to approach the positively charged carbonyl C4 at the glycoaldehyde phosphate. The C2−C4 bond distance is thus chosen as the reaction coordinate, and Figure S6b and Figure 5 plot the energy profiles from the QM(DFT)/MM MD simulations. This bond formation process is exothermic by 24.4 kcal/mol, and the barrier is merely 6.0 kcal/mol. The examination of the conformational evolution along the reaction process, interestingly, reveals that again a couple of proton transfers have occurred. At the transition state with C2−C4 bond distance still quite longer than a normal single bond (**TS4**, see Figure 7), the proton of the hydroxyl group at C2 is already transferred to O4. This proton transfer leaves C4 partially positively charged and thus facilitates the formation of C2−C4 as C2 is negatively charged. As such, a steep decreasing of energy is observed with the shortening of the C2−C4 distance. Along the way, another proton transfer, from the protonated Glu231 to the now negatively charged hydroxyl anion O2, as shown by the snapshot of the product, 2-*C*-methylerythrose 4-phosphate, in Figure 7b.

As **TS4** is a state of the highest energy in the whole reaction cycle, it is valuable to gain more details into the substrate−enzyme interactions. Figure 7a plots the effective hydrogen bonding (<2 Å) of surrounding amino acids and solvent molecules with the forming 2-*C*-methylerythrose 4-phosphate. Apart from the metal ion and the protonated Glu231, which is transferring its proton to O2, there are only a couple of amino acids (i.e., Asn227 and Lys228) interacting with the phosphate group. Each oxygen atom of the phosphate group interacts with two water molecules. This suggests that the product, 2-*C*-methylerythrose 4-phosphate, is ready to exit from the active site and solvate into the solvent. This picture is reinforced by the analyses of the final product configuration **P** as shown in Figure 7b. Lys228 is now moving away, and the negatively charged phosphate group bonds to Gly185 (main-chain NH group), Ser186, Asn227, and a large number of water molecules, while the C4-hydroxyl group interacts with Glu152. The binding between the C2-hydroxyl group and $Mg^{2+}$ is loosened as well (with a distance of 2.48 ± 0.39 Å, as shown in Table S1).

In brief, much like the previous C3−C4 bond-breaking step, although we chose the C2−C4 bond distance here as the reaction coordinate and explored the energy change along the formation of this bond, multiproton shuttles occur along the energy profile. In addition to the obvious C−C bond formation, we observed the resumption of the C2−C3 bond from double to single (Figure S4b), as well as the initial proton transfers from the C2-hydroxyl group to the carbonyl O4, followed by from the protonated Glu231 to the hydroxyl oxygen anion group at the C2 site (Figure S8).

## 3. CONCLUSION

The isomerization of DXP to the intermediate 2-*C*-methylerythrose 4-phosphate is the decisive point in the study of DXR which is a novel target for the development of next generation of antibiotics. Two reaction mechanisms have been proposed, but accumulating new experimental evidence favor the retro-aldol/aldol mechanism over the α-ketol mechanism.[28−31] The key difference between these two mechanisms is the timing of the C3−C4 bond breaking and the C2−C4 bond formation. Although the former mechanism suggests that these two processes are stepwise, the latter corresponds to a concerted reaction. Yet experimentally it is challenging to locate the intermediate state or transition state and determine its


DOI: 10.1021/acscatal.5b00079
*ACS Catal.* 2015, 5, 2805−2813

structure. On the basis of extensive combined QM(DFT)/MM MD simulations, we demonstrated that with the heterolytic cleavage of the C3−C4 bond, the fragments of DXP can stably exist in the forms of 1-propene-1,2-diol and the glycoaldehyde phosphate which interact with surrounding amino acids and a few water molecule via effective hydrogen bonds. Thus, the present computations favor the stepwise retro-aldol/aldol mechanism. Significantly, a series of proton transfers are observed in the process and both Glu152 and Glu231 act as the general bases and acids. These proton shuttles effectively facilitate reactions by lowering their activation barriers. For example, for the cleavage of the aliphatic C3−C4 bond, the reaction barrier is merely 8.2 kcal/mol, which is only a tenth of the normal carbon−carbon single bond energy. This is achieved by the sequential proton transfers from the C4-hydroxyl group to O3 and from the protonated Glu152 to O2. For the formation of the C2−C4 bond, similarly, there are proton transfers from the C2-hydroxyl group to O4 and from the protonated Glu231 to the C2-hydroxyl anion. The whole process is slightly exothermic. Figure 8 summarizes the reaction mechanism.

Approximately, if we view the reaction from **R** to **P** as an elementary one, the state of the highest energy, **TS4**, can be regarded as the transition state, and the reaction barrier would be 21.9 kcal/mol, which represents the up limit of the true complex reaction barrier. Koppisch et al.[46] measured the steady-state kinetic constant $k_{cat}$ for the reduction of DXP to MEP catalyzed by EcDXR, which is 116 ± 8 $s^{-1}$ (or 33 $s^{-1}$, most recently demonstrated by Haymond et al.[67]). This is translated to a complex reaction barrier 14.6 (or 15.4) kcal/mol based on Eyring's transition state theory. Our computations thus overestimate the reaction barrier, most probably due to the B3LYP/6-31G(d) theoretical level. Higher theoretical levels with more electron correlations incorporated will improve the computational prediction. Furthermore, in our computations, the quantum tunneling effect is not considered. Inclusion of this effect may also lower the reaction barrier by up to 4 kcal/mol.[68]

Proton-shuttle catalytic mechanisms have been found in numerous enzyme-catalyzed reactions, for example, reactions involving carbanion intermediates,[69] the reversible hydration of $CO_2$ to $HCO_3^-$ and $H^+$ by carbonic anhydrases,[70] the removal of acetyl moieties from histone tails by histone deacetylases,[71−73] lipase catalyzed *N*-acylation of amino alcohols,[74] and the hydroperoxylation or hydroxylation mechanism of hydroxyethylphosphonate dioxygenase.[75] Our present QM-(DFT)/MM molecular dynamics simulations confirmed the highly efficient aliphatic carbon−carbon bond cleavage and formation induced by the proton shuttles in DXR, where in total there are six proton transfers involved in a complete reaction cycle.

## ■ ASSOCIATED CONTENT

### Supporting Information

The following file is available free of charge on the ACS Publications website at DOI: 10.1021/acscatal.5b00079.

Bonding distances of major ligands to the central metal ion ($Mg^{2+}$) at the key states along the isomerization process, energy profiles for the stepwise isomerization of DXP, snapshots of key structures, and the evolutions of key bond distances along the reaction (PDF)

## ■ AUTHOR INFORMATION


### Corresponding Authors

*E-mail: ymo@wmich.edu (Y.M.).
*E-mail: wurb3@mail.sysu.edu.cn (R.W.).
*E-mail: zxcao@xmu.edu.cn (Z.C.).


### Notes

The authors declare no competing financial interest.

## ■ ACKNOWLEDGMENTS

This work was supported by the U.S. National Science Foundation under Grant CHE-957201 (to H.Y. and Y.M.) and CNS-1126438 (to Y.M.), and the National Science Foundation of China (21203257, 21272289, to R.W.). Z.C. acknowledges the support from the National Science Foundation of China (21133007 and 21373164) and the Ministry of Science and Technology (2011CB808504). We thank the National Supercomputing Centers in Shenzhen and Guangzhou for providing the computational resources.

## ■ REFERENCES


(1) Zhao, L. S.; Chang, W. C.; Xiao, Y. L.; Liu, H. W.; Liu, P. H. *Annu. Rev. Biochem.* **2013**, *82*, 497−530.
(2) Rohmer, M.; Knani, M.; Simonin, P.; Sutter, B.; Sahm, H. *Biochem. J.* **1993**, *295*, 517−524.
(3) Schwarz, M. K. Ph.D. Dissertation, ETH Zürich, Zürich, Switzerland, 1994.
(4) Broers, S. T. J. Ph.D. Dissertation, ETH Zürich, Zürich, Switzerland, 1994.
(5) Takahashi, S.; Kuzuyama, T.; Watanabe, H.; Seto, H. *Proc. Natl. Acad. Sci. U. S. A.* **1998**, *95*, 9879−9884.
(6) Eisenreich, W.; Bacher, A.; Arigoni, D.; Rohdich, F. *Cell. Mol. Life Sci.* **2004**, *61*, 1401−1426.
(7) Kuzuyama, T.; Seto, H. *Nat. Prod. Rep.* **2003**, *20*, 171−183.
(8) Ershov, Y. V. *Appl. Biochem. Microbiol.* **2007**, *43*, 115−138.
(9) Yajima, S.; Nonaka, T.; Kuzuyama, T.; Seto, H.; Ohsawa, K. *J. Biochem.* **2002**, *131*, 313−317.
(10) Proteau, P. J. *Bioorg. Chem.* **2004**, *32*, 483−493.
(11) Hunter, W. N. *J. Biol. Chem.* **2007**, *282*, 21573−21577.
(12) Henriksson, L. M.; Bjorkelid, C.; Mowbray, S. L.; Unge, T. *Acta Crystallogr., Sect. D: Biol. Crystallogr.* **2006**, *62*, 807−813.
(13) Henriksson, L. M.; Unge, T.; Carlsson, J.; Åqvist, J.; Mowbray, S. L.; Jones, T. A. *J. Biol. Chem.* **2007**, *282*, 19905−19916.
(14) MacSweeney, A.; Lange, R.; Fernandes, R. P.; Schulz, H.; Dale, G. E.; Douangamath, A.; Proteau, P. J.; Oefner, C. *J. Mol. Biol.* **2005**, *345*, 115−127.
(15) Reuter, K.; Sanderbrand, S.; Jomaa, H.; Wiesner, J.; Steinbrecher, I.; Beck, E.; Hintz, M.; Klebe, G.; Stubbs, M. T. *J. Biol. Chem.* **2002**, *277*, 5378−5384.
(16) Ricagno, S.; Grolle, S.; Bringer-Meyer, S.; Sahm, H.; Lindqvist, Y.; Schneider, G. *Biochim. Biophys. Acta, Proteins Proteomics* **2004**, *1698*, 37−44.
(17) Steinbacher, S.; Kaiser, J.; Eisenreich, W.; Huber, R.; Bacher, A.; Rohdich, F. *J. Biol. Chem.* **2003**, *278*, 18401−18407.
(18) Yajima, S.; Hara, K.; Iino, D.; Sasaki, Y.; Kuzuyama, T.; Ohsawa, K.; Seto, H. *Acta Crystallogr., Sect. F: Struct. Biol. Cryst. Commun.* **2007**, *63*, 466−470.
(19) Yajima, S.; Hara, K.; Sanders, J. M.; Yin, F.; Ohsawa, K.; Wiesner, J. *J. Am. Chem. Soc.* **2004**, *126*, 10824−10825.
(20) Deng, L.; Endo, K.; Kato, M.; Cheng, G.; Yajima, S.; Song, Y. *ACS Med. Chem. Lett.* **2011**, *2*, 165−170.
(21) Schramm, V. L. *Arch. Biochem. Biophys.* **2005**, *433*, 13−26.
(22) Singh, N.; Cheve, G.; Avery, M. A.; McCurdy, C. R. *Curr. Pharm. Des.* **2007**, *13*, 1161−1177.
(23) Arigoni, D.; Giner, J. L.; Sagner, S.; Wungsintaweekul, J.; Zenk, M. H.; Kis, K.; Bacher, A.; Eisenreich, W. *Chem. Commun.* **1999**, 1127−1128.




DOI: 10.1021/acscatal.5b00079
*ACS Catal.* 2015, 5, 2805−2813

(24) Hoeffler, J. F.; Tritsch, D.; Grosdemange-Billiard, C.; Rohmer, M. *Eur. J. Biochem.* **2002**, *269*, 4446−4457.
(25) Fox, D. T.; Poulter, C. D. *J. Org. Chem.* **2005**, *70*, 1978−1985.
(26) Arigoni, D.; Sagner, S.; Latzel, C.; Eisenreich, W.; Bacher, A.; Zenk, M. H. *Proc. Natl. Acad. Sci. U. S. A.* **1997**, *94*, 10600−10605.
(27) Rohmer, M.; Seemann, M.; Horbach, S.; BringerMeyer, S.; Sahm, H. *J. Am. Chem. Soc.* **1996**, *118*, 2564−2566.
(28) Wong, U.; Cox, R. J. *Angew. Chem., Int. Ed.* **2007**, *46*, 4926−4929.
(29) Munos, J. W.; Pu, X.; Mansoorabadi, S. O.; Kim, H. J.; Liu, H.-W. *J. Am. Chem. Soc.* **2009**, *131*, 2048−2049.
(30) Manning, K. A.; Sathyamoorthy, B.; Eletsky, A.; Szyperski, T.; Murkin, A. S. *J. Am. Chem. Soc.* **2012**, *134*, 20589−20592.
(31) Li, H.; Tian, J.; Sun, W.; Qin, W.; Gao, W. Y. *FEBS J.* **2013**, *280*, 5896−5905.
(32) Fox, D. T.; Poulter, C. D. *Biochemistry* **2005**, *44*, 8360−8368.
(33) Lauw, S.; Illarionova, V.; Bacher, A.; Rohdich, F.; Eisenreich, W. *FEBS J.* **2008**, *275*, 4060−4073.
(34) Kuzuyama, T.; Takahashi, S.; Takagi, M.; Seto, H. *J. Biol. Chem.* **2000**, *275*, 19928−19932.
(35) Fernandes, R. P. M.; Phaosiri, C.; Proteau, P. J. *Arch. Biochem. Biophys.* **2005**, *444*, 159−164.
(36) Fernandes, R. P. M.; Proteau, P. J. *Biochim. Biophys. Acta, Proteins Proteomics* **2006**, *1764*, 223−229.
(37) Benkovic, S. J.; Hammes-Schiffer, S. *Science* **2003**, *301*, 1196−1202.
(38) Bruice, T. C. *Chem. Rev.* **2006**, *106*, 3119−3139.
(39) Gao, J. L.; Ma, S. H.; Major, D. T.; Nam, K.; Pu, J. Z.; Truhlar, D. G. *Chem. Rev.* **2006**, *106*, 3188−3209.
(40) Warshel, A. *Annu. Rev. Biophys. Biomol. Struct.* **2003**, *32*, 425−443.
(41) Warshel, A.; Sharma, P. K.; Kato, M.; Xiang, Y.; Liu, H. B.; Olsson, M. H. M. *Chem. Rev.* **2006**, *106*, 3210−3235.
(42) Senn, H. M.; Thiel, W. *Curr. Opin. Chem. Biol.* **2007**, *11*, 182−187.
(43) Martin, F. P.-D.; Dumas, R.; Field, M. J. *J. Am. Chem. Soc.* **2000**, *122*, 7688−7697.
(44) Yin, X.; Proteau, P. J. *Biochim. Biophys. Acta, Proteins Proteomics* **2003**, *1652*, 75−81.
(45) Argyrou, A.; Blanchard, J. S. *Biochemistry* **2004**, *43*, 4375−4384.
(46) Koppisch, A. T.; Fox, D. T.; Blagg, B. S. J.; Poulter, C. D. *Biochemistry* **2002**, *41*, 236−243.
(47) Gordon, J. C.; Myers, J. B.; Folta, T.; Shoja, V.; Heath, L. S.; Onufriev, A. *Nucleic Acids Res.* **2005**, *33*, W368−W371.
(48) Jorgensen, W. L.; Chandrasekhar, J.; Madura, J. D.; Impey, R. W.; Klein, M. L. *J. Chem. Phys.* **1983**, *79*, 926−935.
(49) Cornell, W. D.; Cieplak, P.; Bayly, C. I.; Gould, I. R.; Merz, K. M.; Ferguson, D. M.; Spellmeyer, D. C.; Fox, T.; Caldwell, J. W.; Kollman, P. A. *J. Am. Chem. Soc.* **1995**, *117*, 5179−5197.
(50) Wang, J. M.; Cieplak, P.; Kollman, P. A. *J. Comput. Chem.* **2000**, *21*, 1049−1074.
(51) Hornak, V.; Abel, R.; Okur, A.; Strockbine, B.; Roitberg, A.; Simmerling, C. *Proteins: Struct., Funct., Genet.* **2006**, *65*, 712−725.
(52) Wang, J. M.; Wolf, R. M.; Caldwell, J. W.; Kollman, P. A.; Case, D. A. *J. Comput. Chem.* **2004**, *25*, 1157−1174.
(53) Case, D. A.; Darden, T. A.; Cheatham, I. T. E.; Simmerling, C. L.; Wang, J.; Duke, R. E.; Luo, R.; Walker, R. C.; Zhang, W.; Merz, K. M.; Roberts, B.; Hayik, S.; Roitberg, A.; Seabra, G.; Swails, J.; Götz, A. W.; Kolossváry, I.; Wong, K. F.; Paesani, F.; Vanicek, J.; Wolf, R. M.; Liu, J.; Wu, X.; Brozell, S. R.; Steinbrecher, T.; Gohlke, H.; Cai, Q.; Ye, X.; Wang, J.; Hsieh, M.-J.; Cui, G.; Roe, D. R.; Mathews, D. H.; Seetin, M. G.; Salomon-Ferrer, R.; Sagui, C.; Babin, V.; Luchko, T.; Gusarov, S.; Kovalenko, A.; Kollman, P. A.; *Amber 12*; University of California: San Francisco, 2012.
(54) Ryckaert, J. P.; Ciccotti, G.; Berendsen, H. J. C. *J. Comput. Phys.* **1977**, *23*, 327−341.
(55) Berendsen, H. J. C.; Postma, J. P. M.; Van Gunsteren, W. F.; DiNola, A.; Haak, J. R. *J. Chem. Phys.* **1984**, *81*, 3684−3690.
(56) Shao, Y.; Fusti-Molnar, L.; Jung, Y.; Kussmann, J.; Ochsenfeld, C.; Brown, S. T.; Gilbert, A. T. B.; Slipchenko, L. V.; Levchenko, S. V.; O'Neill, D. P.; Distasio, R. A., Jr.; Lochan, R. C.; Wang, T.; Beran, G. J.; O. Besley, N. A.; Herbert, J. M.; Lin, C. Y.; Van Voorhis, T.; Chien, S. H.; Sodt, A.; Steele, R. P.; Rassolov, V. A.; Maslen, P. E.; Korambath, P. P.; Adamson, R. D.; Austin, B.; Baker, J.; Byrd, E. F. C.; Dachsel, H.; Doerksen, R. J.; Dreuw, A.; Dunietz, B. D.; Dutoi, A. D.; Furlani, T. R.; Gwaltney, S. R.; Heyden, A.; Hirata, S.; Hsu, C.-P.; Kedziora, G.; Khalliulin, R. Z.; Klunzinger, P.; Lee, A. M.; Lee, M. S.; Liang, W.; Lotan, I.; Nair, N.; Peters, B.; Proynov, E. I.; Pieniazek, P. A.; Rhee, Y. M.; Ritchie, J.; Rosta, E.; Sherrill, C. D.; Simmonett, A. C.; Subotnik, J. E.; Woodcock, H. L., III; Zhang, W.; Bell, A. T.; Chakraborty, A. K.; Chipman, D. M.; Keil, F. J.; Warshel, A.; Hehre, W. J.; Schaefer, H. F., III; Kong, J.; Krylov, A. I.; Gill, P. M. W.; Head-Gordon, M. *Phys. Chem. Chem. Phys.* **2006**, *8*, 3172−3191.
(57) Ponder, J. W.; *TINKER: Software Tools for Molecular Design*, version 4.2; Washington University School of Medicin: St. Louis, MO, 2004.
(58) Zhang, Y. K.; Lee, T. S.; Yang, W. T. *J. Chem. Phys.* **1999**, *110*, 46−54.
(59) Zhang, Y. K. *Theor. Chem. Acc.* **2006**, *116*, 43−50.
(60) Beeman, D. *J. Comput. Phys.* **1976**, *20*, 130−139.
(61) Zhang, Y. K.; Liu, H. Y.; Yang, W. T. *J. Chem. Phys.* **2000**, *112*, 3483−3492.
(62) Torrie, G. M.; Valleau, J. P. *J. Comput. Phys.* **1977**, *23*, 187−199.
(63) Vijayaraj, R.; Van Damme, S.; Bultinck, P.; Subramanian, V. *J. Phys. Chem. B* **2012**, *116*, 9922−9933.
(64) Souaille, M.; Roux, B. *Comput. Phys. Commun.* **2001**, *135*, 40−57.
(65) Kumar, S.; Bouzida, D.; Swendsen, R. H.; Kollman, P. A.; Rosenberg, J. M. *J. Comput. Chem.* **1992**, *13*, 1011−1021.
(66) Wong, A.; Munos, J. W.; Devasthali, V.; Johnson, K. A.; Liu, H. W. *Org. Lett.* **2004**, *6*, 3625−3628.
(67) Haymond, A.; Johny, C.; Dowdy, T.; Schweibenz, B.; Villarroel, K.; Young, R.; Mantooth, C. J.; Patel, T.; Bases, J.; San Jose, G.; Jackson, E. R.; Dowd, C. S.; Couch, R. D. *PLoS One* **2014**, *9*, e106243.
(68) Garcia-Viloca, M.; Gao, J.; Karplus, M.; Truhlar, D. G. *Science* **2004**, *303*, 186−195.
(69) Kim, K. S.; Oh, K. S.; Lee, J. Y. *Proc. Natl. Acad. Sci. U. S. A.* **2000**, *97*, 6373−6378.
(70) Becker, H. M.; Klier, M.; Schüler, C.; McKenna, R.; Deitmer, J. W. *Proc. Natl. Acad. Sci. U. S. A.* **2011**, *108*, 3071−3076.
(71) Corminboeuf, C.; Hu, P.; Tuckerman, M. E.; Zhang, Y. K. *J. Am. Chem. Soc.* **2006**, *128*, 4530−4531.
(72) Wu, R.; Wang, S.; Zhou, N.; Cao, Z.; Zhang, Y. K. *J. Am. Chem. Soc.* **2010**, *132*, 9471−9479.
(73) Chen, K.; Zhang, X.; Wu, Y.-D.; Wiest, O. *J. Am. Chem. Soc.* **2014**, *126*, 11636−11643.
(74) Syrén, P.-O.; Le Joubioux, F.; Ben Henda, Y.; Maugard, T.; Hult, K.; Graber, M. *ChemCatChem* **2013**, *5*, 1842−1853.
(75) Du, L.; Gao, J.; Liu, Y.; Zhang, D.; Liu, C. *Org. Biomol. Chem.* **2012**, *10*, 1014−1024.


DOI: 10.1021/acscatal.5b00079
*ACS Catal.* 2015, 5, 2805−2813